The state-of-the-art and emerging design approaches of double-tuned RF coils for X-nuclei, brain MR imaging and spectroscopy: A review

Chang-Hoon Choi[1,*], Suk-Min Hong[1], Jörg Felder[1], N. Jon Shah[1,2,3,4]

Abstract

With the increasing availability of ultra-high field MRI systems, studying non-proton nuclei (X-nuclei), such as ^{23}Na and ^{31}P has received great interest. X-nuclei are able to provide insight into important cellular processes and energy metabolism in tissues and by monitoring these nuclei closely it is possible to establish links to pathological conditions and neurodegenerative diseases. In order to investigate X-nuclei, a well-designed radiofrequency (RF) system with a multi-tuned RF coil is required. However, as the intrinsic sensitivity of non-proton nuclei is lower compared to ^{1}H, it is important to ensure that the signal-to-noise ratio (SNR) of the X-nuclei is as high as possible.

This review aims to give a comprehensive overview of previous efforts, with particular focus on the design concept of multi-tuned coils, predominantly for brain applications. In order to guide the readers, the main body of the review is categorised into two parts: state-of-the art according to the single or multiple design structures and emerging technologies. A more detailed description is given in each subsection relating to the specific design approaches of, mostly, double-tuned coils, including using traps, PIN-diodes, nested and metamaterial, together with explanations of their novelties, optimal solutions and trade-offs.

1. Introduction

The development of ultra-high field MRI and its increasing availability is advantageous to a number of MR research fields [1,2]. One emerging topic to benefit substantially from the increased signal-to-noise ratio (SNR) offered by ultra-high field systems is the investigation of X-nuclei (non-proton nuclei), *e.g.* oxygen-17 (^{17}O), florine-19 (^{19}F), sodium-23 (^{23}Na) and phosphorus-31 (^{31}P). X-nuclei research is of great interest as X-nuclei can be used to monitor important biochemical processes and to gain physiological information from tissues [3–5]. For example, sodium is closely involved in the sodium-potassium exchange process across cell membranes and can be used to characterise cell metabolism [6,7]. In another application, the values of intra and extracellular sodium concentration in tissue can provide an indicator of cell viability and changes in a number of pathologies [8,9]. Phosphorus accessed by ^{31}P-MR spectroscopy consists of several metabolites and analysis of these can provide valuable insights relating to tissue energetics and membrane metabolism [10,11]. Moreover, alterations in these metabolites are strongly related to a variety of pathological and neurodegenerative conditions [12–14].

Due to their intrinsically lower *in vivo* tissue concentration of X-nuclei and a lower MR sensitivity compared to ^{1}H as shown in Table 1, studies using X-nuclei strive for any gains in SNR. The nuclear Over-hauser effect (NOE) is a technique that can be used to boost the SNR of, for example, ^{13}C and ^{31}P metabolites, and to increase the spectral fitting accuracy [18–20]. Furthermore, as fast scout imaging and static B0 shimming with X-nuclei are also problematic due to low SNR, the concurrent acquisition of ^{1}H imaging is beneficial. To this end, multi-resonant RF coils are likely to be employed, but designing a well-per-forming coil resonating at even two frequencies is challenging as double tuning the coils always results in decreased SNR compared to their counterpart single-tuned coils. Thus, a trade-off is usually encountered, resulting in some degree of loss in one resonant frequency against smaller losses in the other resonant frequency. With this in mind, well-designed double-tuned coils typically need to take the following requirements into consideration [21–23]: 1) highest achievable SNR and efficiency with no coverage penalty, 2) no geometrical/mechanical restrictions, 3) minimum coupling between channels and nuclei-of-interest, 4) no functionality (*e.g.* linear and quadrature drive) or flexibility (*e.g.* multi-channel extension) degradation.

* Corresponding author at: Institute of Neuroscience and Medicine - 4, Forschungszentrum Juelich, 52425 Juelich, Germany.
E-mail address: c.choi@fz-juelich.de (C.-H. Choi).

[1] Institute of Neuroscience and Medicine - 4, Forschungszentrum Juelich, Juelich, Germany
[2] Institute of Neuroscience and Medicine - 11, JARA, Forschungszentrum Juelich, Juelich, Germany
[3] JARA - BRAIN - Translational Medicine, Aachen, Germany
[4] Department of Neurology, RWTH Aachen University, Aachen, Germany

Table 1
MR properties of most commonly used, MR-interesting nuclei in biological tissue [5,15–17].

Nucleus	Gyromagnetic ratio (MHz/T)	Larmor frequency at 7 T (MHz)	Natural abundance (%)	Relative sensitivity to ^{1}H (%)
^{1}H	42.58	298.06	99.985	100
^{3}He	32.43	227.01	0.00014	0.000057
^{13}C	10.72	75.04	1.108	0.0177
^{17}O	−5.77	40.39	0.038	0.00011
^{19}F	40.05	280.35	100	83.3
^{23}Na	11.27	78.89	100	9.25
^{31}P	17.25	120.75	100	6.64
^{35}Cl	4.18	29.26	75.53	0.47
^{39}K	1.83	12.81	93.258	0.0475
^{129}Xe	11.78	82.46	26.44	0.57

The achievement of maximum sensitivity on both channels of a double-tuned coil is an ideal goal and, in light of this, various factors need to be considered, of which, sensitivity is certainly one of the most essential. In practice, achieving optimum sensitivity on both the ^{1}H and X-nucleus channels is difficult and always involves trades-offs since the sensitivity of each counter-part single-tuned coil should be higher than that of the double-tuned coil. Moreover, the use of a single-tuned coil specific to the required purpose always gives better sensitivity. Since optimising sensitivity can be subjective, it is always dependent on its purpose of use and how it is compared. Consequently, it is only possible to achieve optimum sensitivity, for example, if the meaning of optimisation for the ^{1}H channel is limited to standard experiments within a reasonable time, with the X-nucleus channel achieving the best possible sensitivity. This can be an example of an optimisation step, but to advance the coil, one can also make an assumption regarding the technical points by focusing on, for instance, homogeneity or multiple frequencies (e.g. more than two). In an effort to achieve the most optimal trade-off for the planned applications, a large number of approaches have been proposed and demonstrated in recent decades.

This review provides an overview of the key features of previous efforts to design multi-tuned RF coils and give an outlook on emerging technologies. The main body of the review (state-of-the-arts section) is divided into two parts based on the design structures: 1) single-coil configuration and 2) multi-coil configuration. Each section comprises the novel ideas and techniques used for multi-tuning, which includes a) the use of passive elements, b) the use of active switches, c) the use of geometrical decoupling achievements, or d) other novel approaches. This review mostly focuses on designs for brain applications. However, these may also be applicable to other parts of the body. In the subsequent sections, a more detailed description of the specific design approaches of the double-tuned coils is given together with explanations of their novelties, optimal solutions and trade-offs. Peer-reviewed, published articles were used as the main source of this review paper. Conference proceedings and patents were also cited where necessary to amend and compete the information presented in peer-reviewed form.

2. State-of-the-art

2.1. Single-structure approach

The coils introduced in this section operate at two or more different frequencies within a single physical conductor structure. This is achieved by using various techniques. The main advantage of using this single-structure configuration is that it guarantees that the same imaging region will be scanned, thus enabling a straightforward post-acquisition image co-registration. Furthermore, by maintaining isolation among different nuclei, this configuration can be easily extended to the multi-channel array design.

2.1.1. Frequency splitting trap

This is a traditional approach and was popular in the 1980s and early 1990s [24–33]. As shown in Fig. 1, the trap circuit, in principle, divides one resonance frequency into two: one being lower and the other higher. The traps can be designed using a combination of inductor (s) – L and capacitor(s) – C, such as LC (L and C are combined in parallel) and LCC (C is added in series to the L in the LC trap). By adding these traps to each rung or at every loop in the coil, it is possible to generate double- or triple-resonance. However, due to a loss as a result of inserting the trap components, the quality and SNR of the coil are degraded, the extent to which mostly depends on the value of the selected inductor. In general, a 25 to 30% loss in SNR is anticipated when it is compared to the single-tuned coil, but the degree of loss can be managed by the selection of the inductance of the trap as shown in Fig. 1(c) [32]. In other words, the quality of the non-proton coil can be improved by sacrificing that of the ^{1}H coil.

An advantage of using this design is that there is no need to consider interference between the ^{1}H and X-nucleus as the coil resonates at two frequencies within one structure. This means that the B1 field of the coil is intrinsically decoupled with sufficient isolation between the two resonant modes, making it easier to extend a single-channel coil to a multi-channel array coil. However, it may be difficult to implement this approach for applications with close frequencies, *e.g.* ^{1}H/^{19}F or ^{13}C/^{23}Na. Therefore, due to the sensitivity loss, this approach is more

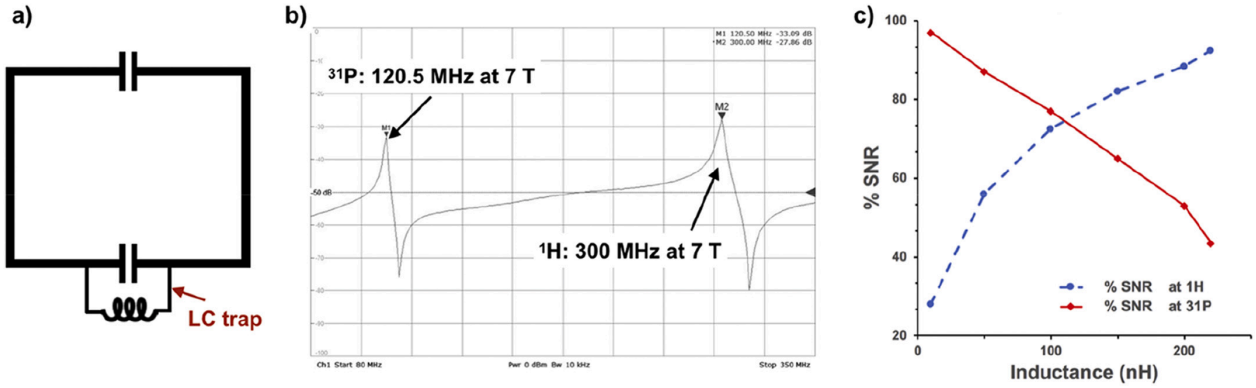

Figure 1. An example of using a frequency splitting trap. The figure shows a simplified loop structure including the trap (a) and its response (b) measured on a networkanalyser (S21) using a double pick-up probe. Fig. (b) shows two resonance peaks tuned to the desired resonance frequencies. In this example, 300 MHz for ^{1}H and 120.5 MHz for ^{31}P at 7 T are shown. The graph (c) shows the effect on SNR for ^{1}H and ^{31}P as a result of the chosen trap inductance at 1.5 T. This figure has been redrawn based on the reference [27] with the copyright permission granted through RightsLink®.

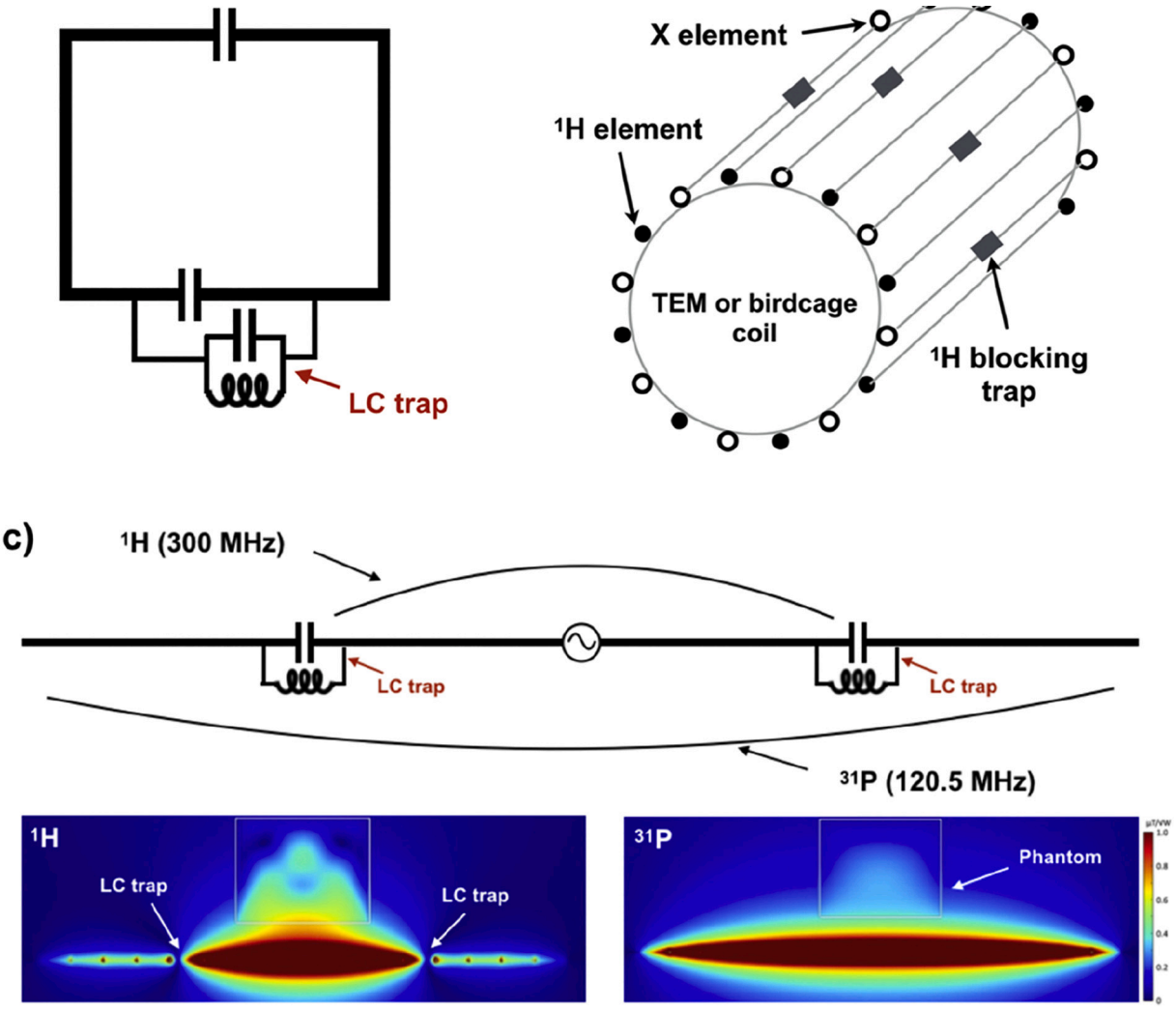

Figure 2. Examples of double-tuned coil designs using blocking traps to suppress ^{1}H current flow in a part of a single physical conductor structure or of a lumped element circuit. The blocking trap is inserted into the simplest loop coil (a) and into an alternating rung resonator of a birdcage or a TEM coil (b). The parallel trap circuits can also be added to each rung to block the other frequency, *e.g.* ^{1}H tuned rung with a ^{13}C blocking trap (not shown). Similarly, the traps can also be included in every element of the dipole antenna array (c). The effect of the trap is obviously seen in the simulated B_1 distribution maps in c) bottom. The original antenna designed for a 9.4T system [39] was re-simulated at 7T. Due to the ^{1}H blocking traps, the ^{1}H current does not flow further to the outside, while the ^{31}P current passes through the trap.

likely to be used for designing double-tuned, transmit-only coils to be used in combination with a single-tuned, multi-channel, receive-only array [33] where the SNR of transmit-only coil is less critical compared to the receive coil, and the loss in transmit coil efficiency can somehow be compensated by the high-power RF amplifiers.

2.1.2. Frequency blocking trap for single-structure

Instead of separating the resonance frequency in two, the traps can also be used to block unwanted frequencies in a single-structure [34–39]. The blocking efficiency, accompanied by insertion loss, is a key factor to be considered when evaluating the quality of this idea. Applying this concept at high-field has become popular, along with deployment of radiating antennas. At the field strengths of ~3T or lower, employing these band-stop traps are more frequently used to the multi-structure coils and the setting-up of two frequencies is readily carried out since both can be controlled independently. Further details relating to the use of blocking traps in a multi-structure will be described in Section 2.2.3.

The trap circuits can be alternatively placed (Fig. 2b) in each lower frequency line of transverse electromagnetic (TEM)-style [37,38] coils to prevent ^{1}H current flowing through that route. This concept can also be employed to the construction of whole-volume birdcages coils [35,36] or surface [34] coils, but in the case of the birdcage designs, the traps are attached to every rung; a lower (higher) frequency trap to the higher (lower) frequency rung. These approaches, however, degrade sensitivity and require the number of the rungs to be doubled in order to maintain B_1 homogeneity, which can be improved using the approach discussed in Section 2.1.5. (See Fig. 5.)

Likewise, the traps can also be used in the single-structure of a dipole antenna (Fig. 2c). The resonance frequency of the dipole antenna is known to be determined by its physical length [40], and, therefore, the length of the dipole antenna required for non-proton nuclei is always longer than that required for ^{1}H. By inserting the band-stop traps as shown in Fig. 2c, ^{1}H current can be trapped while ^{31}P current can go through the traps enabling double-resonance in one antenna [39,41]. The images at the bottom of Fig. 2c are B_1 distribution maps at 7T which were simulated using CST Studio Suite (CST AG, Darmstadt Germany). This indicates that the antenna is tuned to both ^{1}H and ^{31}P

and clearly shows the effect of the traps, *i.e.* ^{1}H current is isolated between the two traps, while ^{31}P current flows through the traps.

2.1.3. PIN-diode or active components

In MRI setups, PIN-diodes function as an electrically controlled switch for the RF and are commonly used to control active detuning units in separate transmit and receive (T/R) coils and T/R switches [42,43]. They are also used to switch a range of resonance frequencies for double, triple or more resonances [44]. Most MRI scanners are equipped with PIN-diode drivers so that the required DC bias can be sufficiently supplied. A PIN-diode works as a conductor, with the presence of a small resistance when forward biased and a high resistance when reverse biased. Due to the resistance of the PIN-diode, as well as the generation of noise within the diode (*e.g.* shot, flicker and Johnson)[45], the sensitivity of a PIN-diode controlled RF coil is diminished, especially, when forward bias is applied. According to Choi et al. [46] and Lim et al. [47] reported SNR losses of approximately 35% in one nucleus when using PIN-diode switches (tuned on) compared to the single-tuned reference coil. Conversely, when it is operating with a reverse voltage, loss because of PIN-diode insertion can be negligible but the degree of power applied is limited because of the reverse breakdown voltage of PIN-diodes [48], resulting in, for example, maladjustment of the transmit power calibration and flip angle.

A number of double-tuned coils using PIN-diodes have been demonstrated and work by shifting the tuning of the circuit to the lower frequency using capacitors [44, 47, 49–51] and to the higher frequency using inductors as shown in (Fig. 3) [46, 52]. Since the Larmor frequencies of the non-proton nuclei mostly used in MR are always lower than ^{1}H, capacitors are more likely to be added in series with the PIN-diodes and act to switch the tuning to the non-proton frequencies. However, this is problematic because the sensitivity of the X-nuclei is already much lower (shown in Table 1) compared to ^{1}H sensitivity and additional losses are not desirable. Therefore, the latter switching approach (using inductors) is preferable, assuming that the PIN-diodes can hold the power.

Building double-tuned coils using PIN-diodes is also particularly useful for applications with nuclei whose resonant frequencies are close, *e.g.* ^{1}H and ^{19}F or among ^{13}C, ^{23}Na and ^{129}Xe, meaning that the use of traps is not practicable due to the finite Q of the trap circuit. It is also beneficial for the multi-channel Rx-only array extension. However, as this requires a multiple DC bias lines, organisation of the bias lines, *e.g.* using a cable bundle and sharing a common ground point is necessary in order to avoid creating ground loops, feeding unwanted noise and coupling to the RF elements. By adding more PIN-diode switching units, the extension to more frequencies is feasible, although the trade-off here is a degradation in the coil quality. However, in recent years, the quality and power handling of the non-magnetic PIN-diode has been improved, resulting in tangible benefits to performance.

As an alternative to PIN-diodes, varactor-diodes [53,54] and micro-electro-mechanical system (MEMS) [55,56] switches can function in a similar way. Moreover, the varactor-diodes are even capable of controlling the capacitance of the tuned circuit by adjusting the applied voltage to the diode. In previous works, this has been employed to tune and match the coil to the desired condition automatically [53,54]. Unlike PIN-diodes and varactor diodes, the MEMS switches are suitable for use in applications requiring higher power.

Rather than using the aforementioned switches, while aiming to increase capacitance on the coil, Pratt et al. designed a double-tuned coil utilising manually-operating mechanical switches [57]. Although the quality of the coil depends highly on the robustness of the mechanical connection, it provides minimum loss on the coil and all other benefits of using double-tuned coils, such as co-registration and shimming.

Recently, the concept of a fluidically tuneable coil has been introduced which uses an amount of fluid containing a high dielectric constant to control tuning and matching of an MTL resonator [58]. However, these require manual operation to switch the tuning during the measurements.

Finally, it should be noted that all double-tuned coils generated by means of switches are not suitable for use in, for example, ^{13}C and ^{31}P experiments using a ^{1}H-decoupled technique which requires RF irradiation of ^{1}H during the measurement.

2.1.4. Four-ring birdcage

The four-ring approach includes two additional end-ring blocks on both sides of a conventional birdcage coil structure. Thus, a single physical structure that supports one current distribution for the generation of a homogeneous RF field is modified to support two modes that can be used for spin system excitation and MR signal reception. By doing so, the coil can be tuned at two different frequencies, one mainly coming from the outer structure and the other from the inner structure [59].

Fig. 4 displays a schematic diagram of a four-ring birdcage coil, the B_1 field patterns generated by each structural block and the coil's characteristics as measured by S_{11}. As the inner/outer structure is low-pass/high-pass, respectively, the lowest resonant frequency is the dominant mode for the inner, while the 2nd from the highest frequency, after the end-ring mode, is the main mode for the outer structure [60]. Both provide a uniform B_1 at the predetermined region of interest, including at the isocentre of the coil. Several configurations of the four-ring birdcage can be used, such as low-pass for both inner and outer, or low-pass for inner and high-pass for outer [61]. The inner part tends to be set to the more important nucleus in the study (therefore, X rather than ^{1}H) and a low-pass configuration is more frequently employed [62].

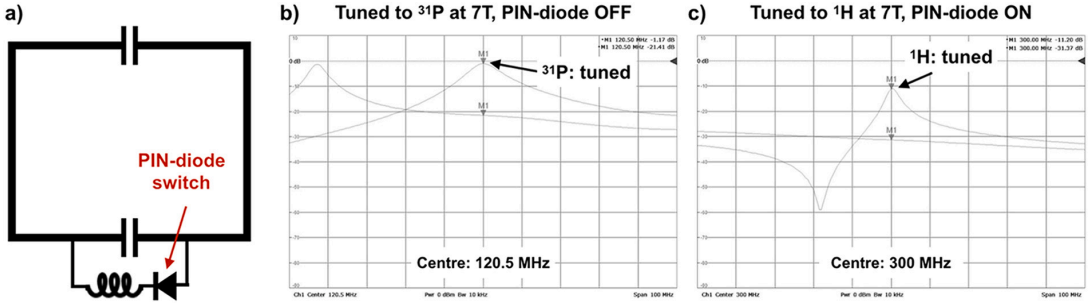

Figure 3. A simplified loop structure using a non-magnetic PIN-diode switch. In this example, the PIN-diode with an inductor in series is inserted in parallel to one of the tuning capacitors in the loop (a). This circuit with the inductor can shift the target resonance frequency upwards when a forward current is applied. A capacitor, instead of the inductor, can also be used to shift the frequency downward. The screen-captured figures b) and c) demonstrate the coil's response measured on a network analyser (S21) using a double pick-up probe. Both display the resonance peak tuned by switching the PIN-diode to each desired resonance frequency: 300 MHz for ^{1}H and 120.5 MHz for ^{31}P at 7T.

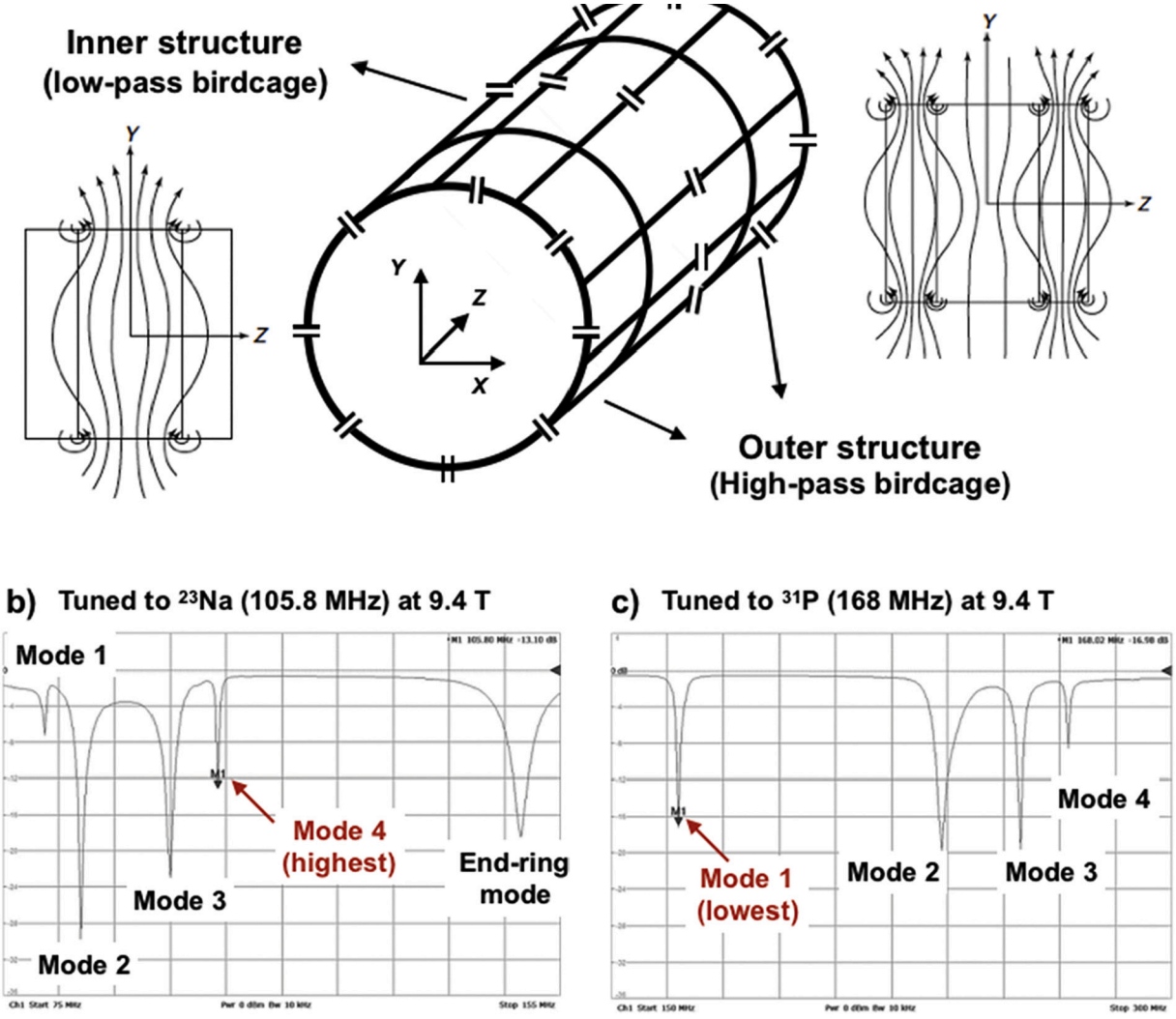

Figure 4. An eight-rung, four-ring birdcage, double-tuned coil. In this example, the low-pass configuration is used for inner structure, tuned to the ^{31}P frequency (168 MHz) at 9.4T, and the high-pass is used for the outer structure, tuned to ^{23}Na (105.8 MHz). This configuration of a type of birdcage coil can be varied, *e.g.* low-pass/low-pass, high-pass/high-pass, low-pass/high-pass, and so on. The B_1 field distributions (a) to the corresponding structures are shown, and the responses of the four-ring birdcage (b and c) are displayed. These were measured on the bench using S_{11}. a) is redrawn based on the reference [59] with the copyright permission granted through RightsLink®.

Four-ring birdcage coils are generally employed as volume coils. An advantage of using a four-ring design is that it does not contain additional lossy components, therefore, it maintains its efficiency an d sensitivity at both frequencies with less than 5% loss at 1.5T [59]. Moreover, it has been reported that, compared to the performance of alternating rung birdcages containing traps, the four-ring birdcage coil is preferred as it offers a higher S NR [63, 64]. However, this comes at the expense of requiring an optimised inner and outer rung length ratio [59], which normally causes a substantial increase in overall coil length. The requirement of additional length for the outer end-rings restricts the accessible space, which can be problematic in applications using smaller coils *i.e. in vivo* brain studies but would be workable in whole-body uses [65]. In order to avoid the problem of an impractically long coil length, shortened and folded four-ring designs [66–69] have been introduced. There are several modifications of the four-ring birdcage coil using different o verall c oil s tructures, such as an Al-derman-Grant coil [70], a split birdcage [71], or a helmet-style coil [72].

2.1.5. Different wavelengths or resonant modes without decoupling units

The coils introduced in this subsection are based on the principle that a single antenna can generate several RF wavelengths and resonant modes.

A quadrature birdcage coil is one of the most widely used coils, and the simplest approach for double tuning a volume coil is to rearrange a quadrature mode of the birdcage coil into two separate linear modes by tuning each linear mode to each target frequency, as shown in Figure 5 a. This is particularly useful in close frequency applications as the capacitor values required to tune the double-tuned coil are not significantly different between the two modes [73, 74]. The design offered by Waiczies *et al* employs this knowledge [75] and instead of using physical lumped capacitors, they chose to build the capacitances using the area of overlap in between the copper strips; all rungs have the over-lapping area distributed uniformly but for the feeding rungs either of ^{1}H or ^{19}F, the overlapped regions are adjusted depending on the desired frequency. This is advantageous for coils requiring very low capacitance for use, for example, at ultra-high field. For close frequency applications, a dipole antenna array using its fundamental property of broad-band tuning was also introduced and has been found to be particularly practicable at ultra-high field [76].

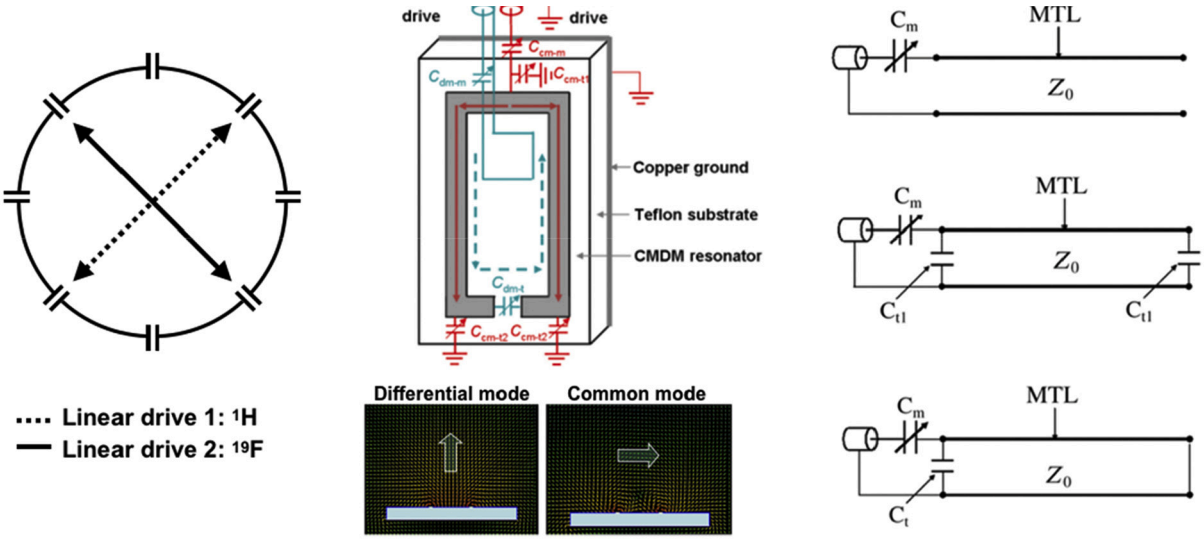

Figure 5. A simplified cross-sectional view of the quadrature birdcage coil in which each linear mode is used to tune to the ^{1}H and ^{19}F frequencies, respectively (a). Due to the way of feeding, the generation of two differential mode and common mode currents is seen (b. top). These provide two intrinsically isolated B_1 fields (b. bottom) so that independent frequency adjustments are allowed. c) is a schematic representation of how the tunings of MTL tuning can be adjusted in different wavelengths, which can eventually be tuned to each nucleus. b) is a reuse of the reference [80] and c) is captured from the reference [86] with the copyright permission granted through RightsLink®.

A surface-mode and butterfly-mode, also known as a common-mode and differential-mode (CMDM), approach for volume [77] and surface [78–80] coils was introduced as a new double-tuned coil design. This design possesses two independent modes with different current paths in a single structure, thus allowing the coil to be operated at two different frequencies with intrinsically decoupled B_1 magnetic fields. For example, in Figure 5b), the current in the two inner loops flows following a figure-of-eight (FO8) coil pattern; generating at ransverse B_1 field (in this case, the common mode), whereas the large outer circle forms as a single loop coil, providing a vertical B_1 field for the differential mode. The selection of these modes is dependent on where the feeding point is. However, an extension of this design to the volumetric or multi-channel array may be limited in this formation.

Although the methods introduced above do not require any extra lossy electrical components to be inserted on the probe structure, they only allow linear driving. The option of discarding the quadrature drive results for both nuclei in a 41% loss of SNR (theoretically but in practice much less), a reduction in RF transmit power efficiency an d th e degradation of B_1 homogeneity [81,82] compared to the quadrature driven coil.

An attempt to use one single low-pass birdcage coil to tune the ^{31}P resonance using the homogeneous mode and the ^{1}H resonance using one of the unused higher modes is described in [83]. In general, the low-pass birdcage coil generates several resonant modes (half of the number of rungs) and among those modes, the lowest mode produces an MR-imageable uniform B_1. This produces high-quality ^{31}P spectra, as it can be as a single-tuned coil, but the quality of ^{1}H imaging was significantly degraded and was only useful for shimming.

This problem can also be overcome by using an alternatingly tuned TEM coil [84,85] as well as a combination of λ/2 and λ/4 wavelength microstrip resonators, as shown in Figure 5c) [86]. By using the advantage of MTL, the wavelength of the resonator can be reconfigured using an identical physical length, that is to say, λ/4 resonators with the same physical length of λ/2 microstrip resonators can operate at a sig-nificantly lower frequency, which is very suitable for tuning to X-nuclei. Consequently, this volume coil is certainly capable of driving the coil in quadrature for both proton and non-proton channels.

Similarly, in a preliminary study, Svejda *et al* have demonstrated results from double-tuned coils designed based on a novel multi-cell composite right-/left-handed (CRLH) metamaterial transmission line method. It was shown that this design could intrinsically generate congeneric current distributions at two frequencies [87–89] from an ordinary right-handed mode (parallel phase) and antiparallel left-handed mode. The resonance behaviour for both frequencies was identical and it was possible to configure the current distribution by altering the termination of the transmission line. In order to achieve a λ/2 distribution, for example, the end of the line must be either short or open. The open end provides a maximum current distribution in the middle of the double-tuned antenna, whereas the short configuration gives current distribution at both ends. Further details of how these particular resonators are built using various types of metamaterials will be given in Section 3.4.

2.2. Multi-structure approach

The coils introduced in this section operate at two or more different frequencies based on two or more separate physical coil structures which are mostly arranged in a geometric fashion so that inductive coupling between the structures can be minimised by using various techniques. The main advantages of the multiple structure configura-tion are 1) an independence of frequency adjustment for the target nuclei is possible and 2) an improvement in SNR – as extra components that give rise to additional losses are not employed. However, it is rather difficult to extend this multi-structure, single-channel coil configuration to a multi-channel array design.

2.2.1. Geometrically decoupled design approach

As shown in Fig. 6, when designing a multi-structure double-tuned coil, one's first instinct may be to simply think about using a geometric decoupling configuration by combining two linearly driven single-tuned coils in an orthogonal direction to each other [90,91], or by overlaying intrinsically different B_1 field propagation, such as either transverse or vertical (perpendicular to the transverse field) B_1 direction [92–102]. Thus, the ^{1}H can be tuned to one frequency and the X-nucleus to the other. This configuration provides roughly the same sensitive volume and

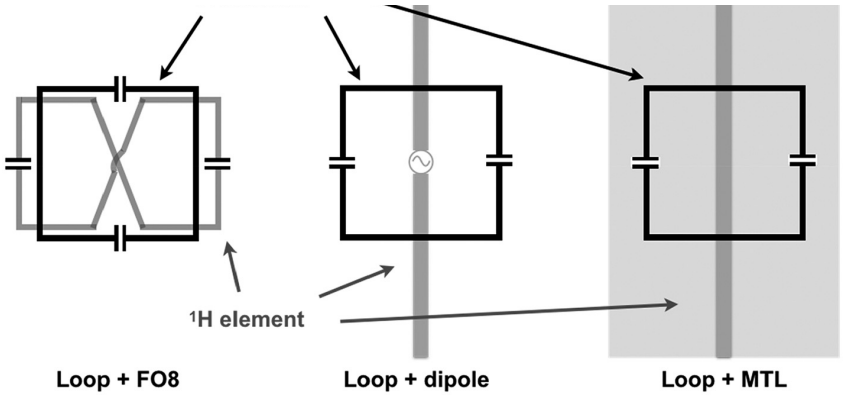

Figure 6. Various geometrical isolated double-tuned coil arrangements. A simple loop structure (vertical B_1 field generating coil) and an FO8 coil (transverse B_1 field generating coil) are overlaid in the best lo-cation to achieve the minimum coupling (a). Each linear coil can be tuned and matched independently from the other coil. The loop coil can be replaced by any other type of coil or antenna generating the vertical B_1 field, *e.g.* solenoid and circular dipole antenna, and the FO8 coil can be replaced by other vertical B_1 field generating probes, *e.g.* MTL, quadrature loop array, monopole and dipole antenna.

the freedom to control both frequencies in-dependently. It also has the advantage of not requiring additional lossy elements. However, unless it is extended to a volume array, it does not offer a quadrature drive, potentially causing degradation in SNR in both the ^{1}H and the X-nuclei channels. This is because, despite B_1 field propagations being geometrically isolated from each other, coupling has to be taken into an account and controlled for.

In a surface coil design, the preferred configuration for use at lower field strengths is a single loop (vertical B_1) with an FO8 or butterfly coil (transverse B_1), whereas a single loop with an MTL monopole or dipole antenna is preferred at higher field strengths. These coil arrangements can be extended to a volumetric transceiver multi-channel array for achieving a homogeneous B_1 field and whole volume coverage or can be used for transmit-only purposes when accompanied with a multi-channel single-tuned (to X-nucleus) receive-only array in order to afford the best possible SNR for X-nuclei [92,103].

In addition, other configurations to improve the performance of the above double-tuned designs have been reported. Choi *et al* developed a quadrature-enhanced coil focusing more on the X-nuclei to improve its quality [97, 98]. Here a mix of loop and butterfly coils were used. By inserting traps or PIN-diodes in the loop, the loop coil was able to re-sonate at two different frequencies, driving the X-nuclei frequency in quadrature and the ^{1}H frequency in linear. Rather than using decou-pling components, Thapa used an additional large loop for ^{1}H and used a quadrature loop/butterfly coil to achieve the same ends [104].

Another configuration of a surface or a half-volume coil design originally shown by Adriany and Gruetter [105], has been used by several groups [106–108]. This design consists of three loops, in which two large loops create a quadrature mode, normally used for the ^{1}H signal, and one small loop for the non-proton signal, is placed in the region where the coupling to the quadrature mode is at a minimum. In this setup, the placement of the small X-nuclei loop and the bending pattern of the quadrature large loops is important as both Schaller *et al* and Li *et al* have reported that they needed to insert decoupling units (traps) to prevent the coupling between the two frequencies [106,108].

An alternative approach to achieving double resonance using a geometrically decoupled design is to tune two separate coils allocated in the two different spaces to each desired frequency. In the case of the ^{1}H signal, a patch antenna operating as a travelling wave resonator [109] positioned just inside the magnet bore (away from the subject) can be used and for the X-nuclei, a single-tuned coil [110] or a single-tuned dialectic resonator [111] can be utilised. This approach is attractive if the focus of the study is mainly on X-nuclei, as any types of existing single-tuned coils can be used for the X-nuclei without any loss other than the quality of the ^{1}H signal, which may just be sufficient enough for scouting and B_0 shimming. Swapping multiple, identical, single-tuned coils between measurements has also been proposed [112, 113]. The benefit of this configuration is that it allows free extension of the choice of nucleus to any nuclei, not only one but to many more without losing any SNR penalty for any selected nuclei since each coil is a single-tuned coil. However, the disadvantage of this system is that it requires the coils to be swapped completely between measurements.

2.2.2. Transformer-coupled, nested arrangement

Since the Fitzsimmons's development of placing a smaller birdcage coil inside a larger one, as shown in Fig. 7a, a transformer-coupled, double-tuned design has been subsequently realised [114–118]. Based on this concept, designs using nested coils have been introduced and modified in various shapes and coil combinations [119–125]. This nested configuration is of particular interest as it has the advantage of not requiring additional lossy elements, thus, in principle, improving the SNR in at least the X-nuclei channel.

In this structure, handling the coupling of the two coil systems is a major mission that impacts significantly on the quality of the ^{1}H signal. It is possible to govern this coupling by amending the distance or ar-rangement of not only between the two coils but also between each channel within one coil, thereby avoiding performance degradation. However, the ability to control the coupling by adjusting the distance between the inner and outer coil may be restricted by the size of the subject and the limited space available inside the magnet bore. To ad-dress this, Galante *et al* have tried to optimise the degree of the rotating angle of one birdcage coil against the other birdcage coil, where both were aligned concentrically, to minimise the coupling between two coils [126].

Nested volume coil arrangements, as developed by Brown *et al*, have positioned both coils in the same plane with half volume shift for minimised coupling, as shown in Fig. 7b [120]. In terms of managing the coupling between next nearest neighbouring elements, Lakshmanan *et al* proposed a triangle-shaped, nested coil array, which was found to improve decoupling among channels for multi-channel array designs. This approach was, in particular, useful for adjusting the coupling between next-nearest neighbour elements since the 1st and 3rd coils are placed close enough to use, for example, a transformer decoupling scheme[127].

Similarly, the combined TEM/birdcage hybrid volume coil designed to achieve double-tuning has been shown to generate uniform B_1 for human brain imaging [128–131]. This configuration is of particular interested since the birdcage is known to be the most used volume coil at medium and lower field strengths (≤ 3T), while TEM is more often used at higher field strengths (> 3T). Thus, the ^{1}H and X-nucleus frequencies can easily be generated by the TEM coil and by the birdcage coil, respectively.

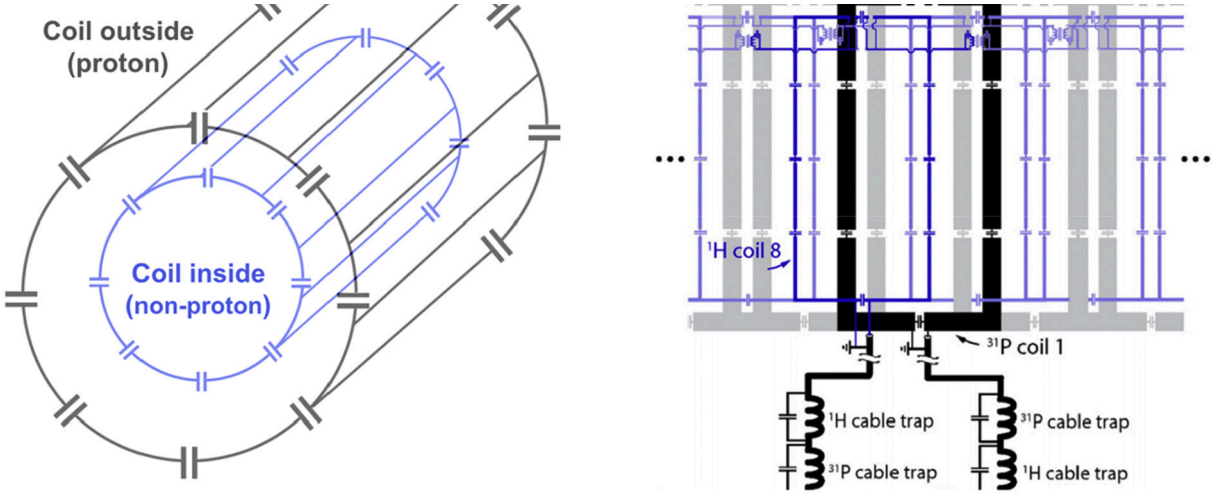

Figure 7. A simplified view of an original transformer coupled double-tuned coil (a) in which two different sized birdcage coils are positioned one inside the other. The one inside possessing superior filling factor is usually tuned to the non-proton frequency. A nested double-tuned coil array (b) is also shown. Two structures containing ^{1}H and ^{31}P elements are overlaid in the same plane. The Fig. 7 b) is captured from the reference [120] with the copyright permission granted through RightsLink®.

In comparison with the double-tuned design that only uses a TEM structure, which struggles in decreased mode splitting at the ^{1}H frequency, this hybrid arrangement has shown a benefit in substantially widened dominant mode separation [130]. However, in terms of coupling between ^{1}H and X frequencies, this design might need sophisticated isolation management as one design by Saha [129] required blocking traps (which is not ideal) between the birdcage and TEM coils, although this was not reported by others [128,130,131].

2.2.3. Frequency blocking trap for multi-structure

As described in the previous Section 2.2, inserting traps to isolate the frequency of one nucleus is a frequently used method to enable a coil to simultaneously operate at more than one resonance frequency. These traps are typically inserted at a lower frequency to block the interference with the high frequency. However, the blocking efficiency is important and some degree of sensitivity reduction in the non-proton channel is unavoidable due to the insertion of traps.

Compared to using the traps in a single structure, the insertion of an LC or LCC trapped second nuclei coil into existing ^{1}H coils is rather popular in the surface coil designs shown in Fig. 8. This has the benefit that, providing that the traps are well optimised, a performance of approximately 90% of their single-tuned, geometrically identical reference coils can be maintained at both frequencies [132–136]. Alecci *et al* [136] built a coil using a conventional LC trap and reported there was an approximately 25% loss in sensitivity for both nuclei, which is higher than that reported by Dabirzadeh *et al* [132]. Optimising the values of the capacitors and inductors is, therefore, a key factor in the minimisation of sensitivity loss. An LCC trap circuit, configured by adding an additional capacitor in series to the inductor in the conventional LC trap, has been also used. This has also been shown to be useful in cases, where the classic LC circuit generally employed for RF coil decoupling could not be used since the required inductance is extremely small to construct, for example, in some ultra-high field and small an-imal coil developments. By using the additional capacitor, the choice of the combination of the component values can be widened further and the required components can be readjusted within a reasonable range [137].

Instead of inserting trap circuits, Brizi *et al* recently designed a double-tuned, $^{1}H/^{23}Na$ coil operating at 7T using tiny spiral resonators (SRs). These were positioned between the inner sodium and outer ^{1}H loops but were not physically connected to either the sodium loop or the ^{1}H loop, thereby minimising any loss due to the insertion of decoupling units. The effectiveness of decoupling between the two nuclei

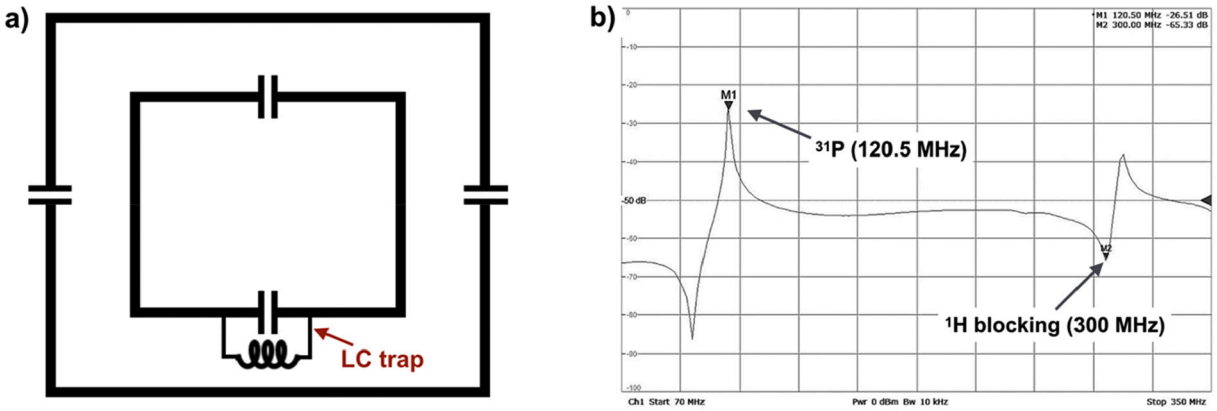

Figure 8. A double-tuned coil using a frequency blocking trap on a multi-structure. A schematic diagram of a pair of concentric loops is shown (a). The inner loop containing the ^{1}H blocking trap is resonated at the ^{31}P frequency and the outer loop at the ^{1}H frequency. As an example, the S_{21} response (b) of the inner loop was measured using a network analyser. Here, the coil was tuned to 120.5 MHz (^{31}P frequency at 7T) while simultaneously blocking 300 MHz (^{1}H at 7T).

was evaluated and the usefulness of the approach was shown [138].

A direct extension of this design to a multi-channel array design is difficult as th e geometry of th e two loops is different, alt hough there have been several volume coils designed using this method [139–141]. In general, the coils with these traps are, therefore, used as a Tx-only coil for X-nuclei (while a ^{1}H coil works for both transmit and receive) in cooperation with a multi-channel receive-only array. Although it is not ideal, there is a way of compensating the tainted efficiency by increasing the output of the high-power amplifiers. Thus, benefits in both SNR improvement using a receive-only array and double-tuning capability can be expected [142,143].

Moreover, Rao *et al* inserted both LC split and LC blocking traps in one loop to tune both ^{3}He and ^{129}Xe frequencies and to isolate the ^{1}H frequency at the same time [144]. By combining this with a ^{1}H coil (extra structure), they were able to carry out triple-nuclei experiments. Building a high-performance, triple-tuned coil is a challenging task. Although the exact value of the losses caused by adding a number of traps was not reported, it is assumed that it resulted in further SNR loss in the triple-tuned coil design [145].

2.2.4. Metamaterial-inspired design

More recently, interest in using metamaterials for MRI has increased. Metamaterials are artificial composite periodic structured materials, which are characterised by the values of effective permittivity and permeability, and offer a unique platform for controlling the propagation of electromagnetic fields [146,147]. The use o f metamaterials has proven to be a promising approach in MRI to boost SNR, particularly at ultra-high field where the RF penetration and B_1 homogeneity are deprived [148–152]. Metamaterials are capable of shaping the main B_1 field distribution of the deeper level efficiently and can be used to enhance SNR and homogeneity in the target regions of interest.

The metamaterial contains one or more conductor paths/ patterns tuned to the appropriate frequencies which can be used to achieve single- or double-tuning, or more. Most of the double-resonant applications using metamaterials are for close frequencies, *i.e.* ^{1}H/^{19}F [153–156]. The double-tuned coil introduced by Hurshkainen *et al* operates at hybridised eigenmodes in two mutually orthogonal periodic structures [14]. In this study, depending on the opted eigenmodes, the field distribution was independently controlled at two close frequencies. One notable advantage of this metamaterial-inspired feeding loop is that it does not need any physical lumped capacitors or inductors for tuning and matching. Furthermore, using a similar technique, Ivanov *et al* demonstrated that the metamaterial-inspired coil could be tuned for a broad range X-nuclei [157]. Vergara Gomez *et al* used two parallel coupled-wire structure to resonate it at the ^{1}H and ^{19}F frequencies. They demonstrated that the SNR of the coil was as high as that of the surface coil and that the coverage was not worse than that of a large birdcage volume coil [155]. Moreover, Yang *et al* utilised an interdigitated capacitive metasurface to show the capability of double-tuning. They positioned this material between the feeding coil and the object and evaluated the B_1 in comparison to that of the single-tuned conventional coil. They observed that the metamaterial inspired double-tuned coil provided a comparable performance for the X-nucleus signal and significant enhancement for the ^{1}H signal [156]. Schmidt and Webb proposed a novel dual-band metamaterial pad, as shown in Fig. 9a. This design combines an electric dipole mode for the X-nuclei (here ^{31}P) frequency and a magnetic dipole mode for the ^{1}H frequency [158]. They constructed multiple patterns in one plane and acquired data from both ^{1}H images and ^{31}P spectra with substantial improvement in SNR – a maximum of 1.8 times higher for ^{31}P and 2.1 times for ^{1}H, as shown in Fig. 9b and c. Despite these clear advantages, using such a metamaterial is a relatively new approach and there are a number of different structures and arrangements to be investigated interms of designing a double- or multi-tuned coil.

3. Outlook and emerging technologies

3.1. Low loss triple- or multiple-tuned coils

By using the techniques reviewed above, it is possible to design coils with the capacity to be tuned at multiple frequencies. However, the question here is, to what extent the quality of the multi-tuned coil can be maintained compared to that of the single-tuned coil as gains in SNR in one frequency are often made to the detriment of another. Even though the exact specifications of the coil design are highly dependent on its actual application and use, the aforementioned literature shows that the use of geometrical decoupling is favoured over the use of the addition of lossy components for double-tuning and enables highly efficient and optimised decoupling circuits. In terms of future developments, it is possible that radiating antennas could be useful for ^{1}H imaging at ultra-high field and further investigation of these may be of interest.

3.2. Double-tuned coils optimised for both ^{1}H and X-nucleus

The ^{1}H signal is not only useful for scout imaging and shimming, but can also be used for functional, high-resolution and multi-parametric imaging. Thus, ignoring the quality of the ^{1}H elements is not ideal. There has been an attempt to build a double-tuned, multi-channel receive-only array coil [33]. However, the coil used a conventional LC split traps could be further improved by using some of the methods introduced in this review.

3.3. Specific absorption rate and temperature monitoring

Within the reference pool accessed for this review paper, only a limited number of articles showing the specific absorption rate (SAR) comparisons between single- and double-tuned coils were available [*e.g.* 39, 73, 123, 143, 159] and any papers describing, for example, the temperature rise related effect where the lumped elements are located, were not found. In terms of overall SAR performance, it was also reported that the severe SAR penalty for most of the designs was not obviously presented in the double-tuned coil in comparison to the single-tuned coil. However, X-nuclei studies are more likely to be carried out at ultra-high field, so investigating SAR or carrying out thermometry experiments of newly designed double-tuned coils is highly recommended.

3.4. Parallel transmit technique

Parallel transmit (pTx) has become a popular technique for ultra-high field human ^{1}H imaging. The fundamental purpose of pTx is to compensate for the problems derived due to the shortened RF wave-length in the tissue at higher field strength (≥ 7T). Similar to 1H, X-nuclei Tx coils, particularly, for ^{19}F imaging would also benefit from the application of the pTx technique since both Larmor frequencies are close each other (*e.g.* 282 MHz for ^{19}F and 300 MHz for ^{1}H at 7T). However, utilising pTx with the other X-nuclei may not be advantageous for head applications at 7T or 9.4T. Evidence to support this comes from the fact that most MR scanners up to 3T are equipped with a ^{1}H body coil, which generates a uniform excitation, and the Larmor frequency of these X-nuclei is similar to or much lower than that of the ^{1}H at 3T (~ 127 MHz). However, beyond 9.4 T pTx may be needed for ^{31}P studies and would also play an important role in offering a uniform B_1 to other X-nuclei investigations. Alternatively, the pTx technique would also allow us to be able to minimise SAR, as shown in Section 3.3, and enables the control of independent Tx channels simultaneously. Consequently, we can potentially (if MR console allows or using a multiband technique) apply a multi-X-frequency excitation and can benefit from employing, for example,

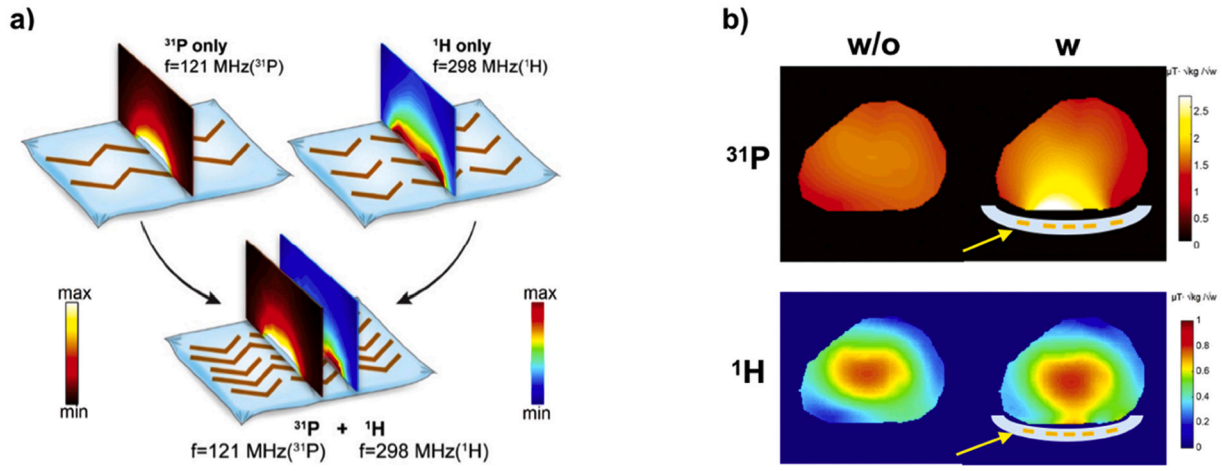

Figure 9. A schematic diagram of a double-tuned, $^{1}H/^{31}P$ metamaterial pad and its characteristic view (a) which combines two different patterned metamaterial structures. Fig. 9b shows the B1+ maps with (w) and without (w/o) the support of the metamaterial pad. The substantial enhancement of efficiencies at both frequencies can be clearly seen with the metamaterial. The Fig. 9 a) is reused and b) is redrawn from the reference (https://pubs.acs.org/doi/10.1021/acsami. 7b06949) [158] with the copyright permission granted from ASC.

^{31}P and ^{23}Na (or any other nuclei) excitation at the same time. This would significantly shorten the overall multinuclear MR acquisition time and may improve temporal resolution. Furthermore, pTx may also improve the efficiency of NOE or ^{1}H-decoupling to further enhance ^{13}C and ^{31}P measurements.

3.5. New decoupling scheme

Decoupling between coil channels is an important topic for both ^{1}H array coils as well as for double-tuned coil designs as it directly affects the coil efficiency, noise and sensitivity loss. Currently, the three most frequently used decoupling methods are: overlap [159], capacitive [160] and inductive decoupling [161]), although, more recently, novel decoupling schemes have been introduced. Zhang et al. and Ruytenberg et al. developed a high-impedance coil design that can eliminate all interactions between elements in a phased array coil [162,163]. Similarly, Yan et al. demonstrated a self-decoupled antenna design by adjusting capacitance distribution on the coil to balance and cancel out magnetic and electric coupling [164]. These techniques even allow excellent isolation between the element and its next nearest neighbours, and flexibility in allocating the coil elements in the array. In addition, induced current elimination decoupling [165,166], magnetic wall de-coupling [167], split-loop resonator on a dense dipole array [168] and metamaterial decoupling [138,169] have also been used to improve decoupling, primarily at UHF. Although, to date, these approaches have mostly been employed to ^{1}H, many of these new methods may also be implementable in the multi-channel, double-tuned coil designs, and this needs further investigation in the future.

3.6. B_0 shimming method using ^{23}Na signal

As mentioned above, the inclusion of a ^{1}H channel is not necessary if the usage of ^{1}H is only for localising images and for the B_0 shimming. Instead, B_0 shimming can be achieved with the use of non-proton signals and has been introduced using the most abundant sodium signals [170]. This is advantageous as it enables a high quality single-tuned ^{23}Na coil to be utilised and requires no decoupling units or complication in the coil structure. Moreover, instead of using the ^{1}H channel, a double-tuned coil can be built in combination with other more meta-bolically and physiologically relevant nuclei, *e.g.* ^{23}Na, ^{35}Cl and ^{39}K [171,172].

3.7. Double-tuned coils for multi-modality

Another challenging aspect of double-resonant coil design is when it is required for use with other imaging modalities, *e.g.* PET, X-ray, Ultrasound or Linac. The specifications of these modalities [173–177] are completely different to those of MR so any classical approach is unlikely to work well. For example, in the case of PET, only low-density materials can be used within an imaging field of view (FOV) which means capacitors, coaxial cables, *etc.* will create unwanted artefacts and photon counting losses [178]. Recently, a double-tuned coil for hybrid MR-PET imaging was introduced by Oehmigen et al. In this design, an existing commercial double-tuned birdcage design was modified by relocating all the dense materials, mostly capacitors into outside the PET FOV [179]. Although the performance of the double-tune coil was successfully optimised for PET, the quality of the MRI is unlikely to be as good as that of the stand-alone MRI, *e.g.* together using a multi-channel receive array. Moreover, the use of parallel imaging is not possible in this design as the double-tuned birdcage coil itself has no receive arrays, and, therefore, it is not the ideal design for some studies. Anazodo *et al* investigated the usefulness of using a coil array pattern based on aluminium instead of using copper [173] and Choi *et al* compared various copper-based RF coil materials to build a double-tuned $^{1}H/^{31}P$ coil for an MR-PET system [180]. Sander *et al* and Farag *et al* evaluated the use of the receive array with PET [181,182], and Choi *et al* compared the performance of various surface coil designs for hybrid MR-PET [183]. These activities are useful in improving the quality of the double-tuned coils used for hybrid MR-PET systems.

4. Summary

Table 2 shows a review of the double-tuned coil designs covered in this paper, along with their associated trade-offs. Note that the evaluation given here is for a comparison between the proposed double-tuned designs and an isolated single-tuned coil and comparisons are not made between the different design approaches.

Table 2
Summary of double-tuned coil designs and their trade-offs.

	Design type	SNR in X	SNR in ^{1}H	Coupling between X and ^{1}H	Multi-channel extension feasibility	Space restricton	Image co-registration	References
Single-structure	Split trap	3	3	4	5	5	5	[24–33]
	Blocking trap	4	4	4	5	4	4	[34–39]
	PIN-diode with capacitor	2	5	5	5	4	5	[47,49–51]
	PIN-diode with inductor	5	2	5	5	4	5	[46,52]
	Manual, mecanical switch	5	5	5	2	4	5	[57]
	Four-ring	4	4	3	*	2	4	[59–72]
	Two linear modes	3	3	4	2	4	4	[73,74]
	CMDM	3	3	4	3	4	4	[77–80]
	λ/2 and λ/4 wavelength	5	5	4	4	3	4	[84–86]
	CRLH	5	5	4	4	3	4	[87–89]
Multi-structure	Geometrical isolation	4	4	4	3	3	4	[90–108,110–113]
	Nested	5	3	3	3	3	4	[114–127]
	TEM/Birdcage	4	4	4	#	3	4	[128–131]
	Blocking trap	4	4	4	3	3	4	[132–145]
	Metamaterial	5	5	3	3	2	4	[153–158]

Scale 1–5, 1: poor and 5: excellent, Note that this evaluation is for the comparison between its counterpart single-tuned coil not among the designs.

* Scoring the four-ring design approach for this category (multi-channel array extension) is excluded since the design is based on a birdcage volume coil.

Scoring this is excluded since the TEM/birdcage is mainly designed as a volume transmit/receive coil.

Declaration of Competing Interest

The authors have no conflicts of interest to declare.

Acknowledgements

The authors thank Ms. Rick for English proofreading. We also acknowledge the reviewers for their constructive comments, as well as Prof. Alecci for his valuable discussion.

References

[1] Kraff O, Fischer A, Nagel AM, Mönninghoff C, Ladd ME. MRI at 7 tesla and above: demonstrated and potential capabilities. J Magn Reson Imaging 2015;41:13–33.
[2] Ladd ME, Bachert P, Meyerspeer M, et al. Pros and cons of ultra-high-field MRI/MRS for human application. Prog Nucl Mag Res Sp 2018;109:1–50.
[3] Hu R, Kleimaier D, Malzacher M, Hoesl MAU, Paschke NK, Schad LR. X-nuclei imaging: current state, technical challenges, and future directions. J Magn Reson Imaging 2020;51:355–76.
[4] Niesporek SC, Nagel AM, Platt T. Multinuclear MRI at ultrahigh fields. Top Magn Reson Imaging 2019;28:173–88.
[5] Worthoff WA, Shymanskaya A, Choi C-H, Felder J, Oros-Peusquens AM, Shah NJ. Multinuclear MR imaging and spectroscopy. In: Cercignani M, Dowell NG, Tofts PS, editors. Quantitative MRI of the Brain. Boca Raton: CRC Press; 2008.
[6] Springer CS. Using 1 H 2 O MR to measure and map sodium pump activity in vivo. J Magn Reson 2018;291:110–26.
[7] Shah NJ, Worthoff WA, Langen K-J. Imaging of sodium in the brain: a brief review. NMR Biomed 2016;29:162–74.
[8] Madelin G, Kline R, Walvick R, Regatte RR. A method for estimating intracellular sodium concentration and extracellular volume fraction in brain in vivo using sodium magnetic resonance imaging. Sci Rep 2015;4:4763.
[9] Fiege DP, Romanzetti S, Mirkes CC, Brenner D, Shah NJ. Simultaneous single-quantum and triple-quantum-filtered MRI of 23Na (SISTINA). Magn Reson Med 2013;69:1691–6.
[10] de Graaf RA, Feyter HMD, Brown PB, Nixon TW, Rothman DL, Behar KL. Detection of cerebral NAD+ in humans at 7T. Magn Reson Med 2017;78:828–35.
[11] Ren J, Sherry AD, Malloy CR. 31P-MRS of healthy human brain: ATP synthesis, metabolite concentrations, pH, and T1 relaxation times. NMR Biomed 2015;28:1455–62.
[12] Stovell MG, Yan JL, Sleigh A, Mada MO, Carpenter TA, Hutchinson PJA, et al. Assessing metabolism and injury in acute human traumatic brain injury with magnetic resonance spectroscopy: current and future applications. Front Neurol 2017;8:642.
[13] Rijpma A, van der Graaf M, Meulenbroek O, Olde Rikkert MGN, Heerschap A. Altered brain high-energy phosphate metabolism in mild Alzheimer's disease: a 3-dimensional 31P MR spectroscopic imaging study. Neuroimage Clin 2018;18:254–61.
[14] Chouinard VA, Kim SY, Valeri L, Yuksel C, Ryan KP, Chouinard G, et al. Brain bioenergetics and redox state measured by 31P magnetic resonance spectros-copy in unaffected siblings of patients with psychotic disorders. Schizophr Res 2017;187:11–6.
[15] de Graaf R. In Vivo NMR Spectroscopy: Principles and Techniques. 2nd ed. Wiley;2007.
[16] de Graaf R. In Vivo NMR Spectroscopy: Principles and Techniques. 3rd ed. Wiley; 2019.
[17] Buonocore MH, Maddock RJ. Magnetic resonance spectroscopy of the brain: a review of physical principles and technical methods. Rev Neurosci 2015;26:609–32.
[18] Ren J, Sherry AD, Malloy CR. Band inversion amplifies 31P–31P nuclear over-hauser effects: relaxation mechanism and dynamic behavior of ATP in the human brain by 31P MRS at 7 T. Magn Reson Med 2017;77:1409–18.
[19] Peeters TH, van Uden MJ, Rijpma A, Scheenen TWJ, Heerschap A. 3D ^{31}P MR spectroscopic imaging of the human brain at 3T with a ^{31}P receive array: An assessment of ^{1}H decoupling, T_1 relaxation times, ^{1}H-^{31}P nuclear Overhauser effects and NAD+. NMR Biomed 2019:e4169. https://doi.org/10.1002/nbm. 4169.
[20] Sailasuta N, Robertson LW, Harris KC, Gropman AL, Allen PS, Ross BD. Clinical NOE 13C MRS for neuropsychiatric disorders of the frontal lobe. J Magn Reson 2008;195:219–25.
[21] Mispelter J, Mikaela L, Briguet A. NMR Probeheads for Biophysical and Biomedical Experiments: Theoretical Principles and Practical Guidelines. 2nd ed. Imperial College Press; 2015.
[22] Vaughan JT, Griffiths JR. RF Coils for MRI. Wiley; 2012.
[23] Felder J, Choi C-H, Shah NJ. Chapter 2: MRI Instrumentation. Hybrid MR-PET Imaging. 2018. p. 45–63.
[24] Zakian KL, Koutcher JA, Ballon D. A dual-tuned resonator for proton-decoupled phosphorus-31 chemical shift imaging of the brain. Magn Reson Med 1999;41:809–15.
[25] Shen GX, Boada FE, Thulborn KR. Dual-frequency, dual-quadrature, birdcage RF coil design with identical B1 pattern for sodium and proton imaging of the human brain at 1.5 T. Magn Reson Med 1997;38:717–25.
[26] Shen GX, Wu JF, Boada FE, Thulborn KR. Experimentally verified, theoretical Design of Dual-Tuned, low-pass birdcage radiofrequency resonators for magnetic resonance imaging and magnetic resonance spectroscopy of human brain at 3.0 tesla. Magn Reson Med 1999;41:268–75.
[27] Schnall MD, Subramanian VH, Leigh JS, Chance B. A new double-tuned probed for concurrent 1H and 31P NMR. J Magn Reson 1985;65:122–9.
[28] Wetterling F, Tabbert M, Junge S, Gallagher L, Macrae IM, Fagan AJ. A double-tuned 1H/23Na dual resonator system for tissue sodium concentration measure-ments in the rat brain via Na-MRI. Phys Med Biol 2010;55:7681–95.
[29] Tadanki S, Colon RD, Moore J, Waddell KW. Double tuning a single input probe for heteronuclear NMR spectroscopy at low field. J Magn Reson 2012;223:64–7.
[30] de Bisschop E, Annaert G, Luypaert R, Coremans J, Osteaux M. Absolute quanti-fication of 31P muscle metabolites using NMRS with an internal standard and a high-Q, double-tuned coil. Biochim Biophys Acta 1991;1094:147–52.
[31] Leach MO, Hind A, Sauter R, Requardt H, Weber H. The design and use of a dual-frequency surface coil providing proton images for improved localization in 31P spectroscopy of small lesions. Med Phys 1986;13:510–3.
[32] Isaac G, Schnall MD, Lenkinski RE, Vogele K. A design for a double-tuned birdcage coil for use in an integrated MRI/MRS examination. J Magn Reson 1990;89:41–50.
[33] Rowland BC, Driver ID, Tachrount M, et al. Whole brain 31P MRSI at 7T with a dual-tuned receive array. Magn Reson Med 2020;83:765–75.

[34] Wetterling F, Högler M, Molkenthin U, Junge S, Gallagher L, Mhairi Macrae I, et al. The design of a double-tuned two-port surface resonator and its application to in vivo hydrogen- and sodium-MRI. J Magn Reson 2012;217:10–8.
[35] Rath R. Design and performance of a double-tuned bird-cage coil. J Magn Reson 1990;86:488–95.
[36] Matson GB, Vermathen P, Hill TC. A practical double-tuned 1H/31P quadrature birdcage head coil optimized for 31P operation. Magn Reson Med 1999;42:173–82.
[37] Durr W, Rauch S. A dual-frequency circularly polarizing whole-bodyMR antenna for 69/170 MHz. Magn Reson Med 1991;19:446–55.
[38] Yahya A, de Zanche N, Allen PS. A dual-tuned transceive resonator for (13) C{(1) H} MRS: two open coils in one. NMR Biomed 2013;26:533–41.
[39] Hong SM, Choi C-H, Felder J, Shah NJ. Design and simulation of dual-band dipole antenna for 1H/31P at 9.4T MRI. Proc Intl Soc Mag Reson Med 2018;26:4400.
[40] Raaijmakers AJ, Luijten PR, van den Berg CA. Dipole antennas for ultrahigh-field body imaging: a comparison with loop coils. NMR Biomed 2016;29:1122–30.
[41] H.K. Morgan. Radio antenna system. US2229865. 1941.
[42] Barberi EA, Gati JS, Rutt BK, Menon RS. A transmit-only/receive-only (TORO) RF system for high-field MRI/MRS applications. Magn Reson Med 2000;43:284–9.
[43] Garbow JR, Mcintosh C, Conradi MS. Actively decoupled transmit–receive coil-pair for mouse brain MRI. Concepts Magn Reson B 2008;33:252–9.
[44] Choi C-H, Hutchison JMS, Lurie DJ. Design and construction of an actively fre-quency-switchable RF coil for field-dependent magnetisation transfer contrast MRI with fast field-cycling. J Magn Reson 2010;207:134–9.
[45] Thompson M. Intuitive Analog Circuit Design. 2nd ed. Newnes; 2013.
[46] Choi C-H, Hong S, Ha Y, Shah NJ. Design and construction of a novel 1H/19F double-tuned coil system using PIN-diode switches at 9.4T. J Magn Reson 2017;279:11–5.
[47] Lim H, Thind K, Martinez-Santiesteban FM, Scholl TJ. Construction and evaluation of a switch-tuned 13C - 1H birdcage radiofrequency coil for imaging the meta-bolism of hyperpolarized 13C-enriched compounds. J Magn Reson Imaging 2014;40:1082–90.
[48] Doherty W, Joos R. The PIN Diode Circuit Designers' Handbook. Watertown: Microsemi Corporation; 1998.
[49] Ha S, Hamamura MJ, Nalcioglu O, Muftuler LT. A PIN diode controlled dual-tuned MRI RF coil and phased array for multi nuclear imaging. Phys Med Biol 2010;55:2589–600.
[50] Voelker MN, Koenig AM, Braun S, Mahnken AH, Heverhagen JT. A PIN-diode-controlled double-tuned birdcage coil for 1H-imaging and 31P-spectroscopy on mice. Proc Intl Soc Mag Reson Med 2013;21:2779.
[51] Han SD, Heo P, Kim HJ, Song H, Kim D, Seo J-H, et al. Double-layered dual-tuned RF coil using frequency-selectable PIN-diode control at 7-T MRI. Concepts Magn Reson B 2017;47:e21363.
[52] Villa-Valverde P, Rodríguez I, Padró D, Benito M, Garrido-Salmon CE, Ruiz-Cabello J. A dual 1H/19F birdcage coil for small animals at 7 T MRI. Magn Reson Mater Phys 2019;32:79–87.
[53] Muftuler LT, Gulsen G, Sezen KD, Nalcioglu O. Automatic tuned MRI RF coil for multinuclear imaging of small animals at 3T. J Magn Reson 2002;155:39–44.
[54] de Alejo RP, Garrido C, Villa P, Rodriguez I, Vaquero JJ, Ruiz-Cabello J, et al. Automatic tuning and matching of a small multifrequency saddle coil at 4.7 T. Magn Reson Med 2004;51:869–73.
[55] Maunder A, Rao M, Robb F, Wild JM. Comparison of MEMS switches and PIN diodes for switched dual tuned RF coils. Magn Reson Med 2018;80:1746–53.
[56] Maunder A, Rao M, Robb F, Wild JM. An 8-element Tx/Rx array utilizing MEMS detuning combined with 6 Rx loops for 19F and 1H lung imaging at 1.5T. Magn Reson Med 2020. https://doi.org/10.1002/mrm.28260.
[57] Pratt R, Giaquinto R, Ireland C, et al. A novel switched frequency 3He/1H high-pass birdcage coil for imaging at 1.5 tesla. Concepts Magn Reson B 2015;45:174–82.
[58] Abuelhaia A, Salma S, El-Absi M. Multi-tuned RF coil using microfluidically tun-able RF capacitor for RMI/MRS at 7T. IRECAP 2019;9:6.
[59] Murphy-Boesch J, Srinivasan R, Carvajal L, Brown TR. Two configurations of the four-ring birdcage coil for 1 H imaging and 1 H-decoupled 31 P spectroscopy of the human head. J Magn Reson 1994;103:103–14.
[60] Hayes EC, Edelstein WA, Schenck JF, et al. An efficient highly homogeneous radiofrequency coil for whole-body NMR imaging at 1.5 T. J Magn Reson 1985;63:622–828.
[61] Murphy-Boesch J. Double-tuned birdcage coils: construction and tuning. Encyclop Magn Reson 2011. https://doi.org/10.1002/9780470034590.emrstm1121.
[62] Lanz T, von Kienlin M, Behr W, Haase A. Double-tuned four-ring birdcage re-sonators for in vivo 31P-nuclear magnetic resonance spectroscopy at 11.75 T. Magn Reson Mat Phys Biol Med 1997;5:243–6.
[63] Lykowsky G, Carinci F, Düring M, Weber D, Jakob PM, Haddad D. Optimization and comparison of two practical dual-tuned birdcage configurations for quanti-tative assessment of articular cartilage with sodium magnetic resonance imaging. Quant Imaging Med Surg 2015 Dec;5(6):799–805.
[64] Tomanek B, Volotovskyy V, Gruwel MLH, Mckenzie E, King SB. Double-frequency birdcage volume coils for 4.7T and 7T. Concepts Magn Reson B 2005;26:16–22.
[65] Boskamp E, Xie Z, Taracila V, Stephen A, Edwards M, Skloss T, et al. A dual-tuned 70 cm whole-body resonator for 13C and proton MRI/MRS at 3T. Proc Intl Soc Mag Reson Med 2018;26:1714.
[66] Duan Y, Peterson BS, Liu F, Brown TR, Ibrahim TS, Kangarlu A. Computational and experimental optimization of a double-tuned 1H/31P four-ring birdcage head coil for MRS at 3T. J Magn Reson Imaging 2009;29:13–22.
[67] Shan K, Duan Y. Rapid four-ring birdcage coil analysis: design optimization for high efficiency, low interference, and improved body loading tolerance. Magn Reson Imaging 2019;66:30–5.
[68] Ha Y, Choi C-H, Worthoff WA, Shymanskaya A, Schöneck M, Willuweit A, et al. Design and in vivo use of a folded four-ring double-resonant quadrature birdcage coil for rat brain sodium imaging at 9.4T. J Magn Reson 2018;286:110–4.
[69] Maggiorelli F, Retico A, Boskamp E, et al. Double tuned 1H-23Na birdcage coils for MRI at 7 T: performance evaluation through electromagnetic simulations. IEEE International Symposium on Medical Measurements and Applications. 2018.
[70] Derby K, Tropp J, Hawryszko C. Design and evaluation of a novel dual-tuned re-sonator for spectroscopic imaging. J Magn Reson 1990;86:645–51.
[71] Potter WM, Wang L, Mccully KK, Zhao Q. Evaluation of a new 1H/31P dual-tuned birdcage coil for 31P spectroscopy. Concepts Magn Reson B 2013;43:90–9.
[72] Hong SM, Choi C-H, Shah NJ, Felder J. Design and evaluation of a (1)H/(31)P double-resonant helmet coil for 3T MRI of the brain. Phys Med Biol 2019;64:035003.
[73] Joseph PM, Lu D. A technique for double resonant operation of birdcage imaging coils. IEEE Trans Med Imaging 1989;8:286–94.
[74] Gajawada G, Li T, Couch MJ, Fox MS, Albert M. A 19F-1H linear dual tuned RF birdcage coil for rat lung imaging at 3T. Proc Intl Soc Mag Reson Med 2015;23:1461.
[75] Waiczies H, Lepore S, Drechsler S, et al. Visualizing brain inflammation with a shingled-leg radio-frequency head probe for 19F/1H MRI. Sci Rep 2013;3:1280.
[76] Van Gorp JS, Seevinck RP, Andreychenko A, et al. 19F MRSI of capecitabine in the liver at 7T using broadband transmit-receive antennas and dual-band RF pulses. NMR Biomed 2015;28:1433–42.
[77] Peshkovsky AS, Kennan RP, Fabry ME, Avdievich NI. Open half-volume quad-rature transverse electromagnetic coil for high-field magnetic resonance imaging. Magn Reson Med 2005;53:937–43.
[78] Pang Y, Zhang X, Xie Z, Wang C, Vigneron D. Common-mode differential-mode (CMDM) method for double-nuclear MR signal excitation and reception at ultra-high fields. IEEE Trans Med Imaging 2011;30:1965–73.
[79] Cao P, Zhang X, Park I, Najac C, Nelson SJ, Ronen S, et al. 1H-13C independently tuned radiofrequency surface coil applied for in vivo hyperpolarized MRI. Magn Reson Med 2016;76:1612–20.
[80] Li Y, Yu B, Pang Y, Vigneron DB, Zhang X. Planar quadrature RF transceiver design using common-mode differential-mode (CMDM) transmission line method for 7T MR imaging. PLoS ONE 2013;8:e80428.
[81] Glover GH, Hayes CE, Pelc NJ, et al. Comparison of linear and circular polarization for magnetic resonance imaging. J Magn Reson 1985;64:255–70.
[82] Chen C-N, Hoult DI, Sank VJ. Quadrature detection coils - a further √2 improve-ment in sensitivity. J Magn Reson 1983;54:324–7.
[83] Webb AG, Smith NB, Aussenhofer S, Kan HE. Use of tailored higher modes of a birdcage to design a simple double-tuned proton /phosphorus coil for human calf muscle studies at 7 T. Concepts Magn Reson B 2011;39:89–97.
[84] Avdievich NI, Hetherington HP. Actively detuneable double-tuned 1 H/31P head volume coil and four-channel 31P phased array for human brain spectroscopy. J Magn Reson 2007;186:341–6.
[85] Vaughan JT, Hetherington HP, Otu JO, Pan JW, Pohost GM. High frequency vo-lume coils for clinical NMR imaging and spectroscopy. Magn Reson Med 1994;32:206–18.
[86] Pang Y, Xie Z, Xu D, Kelley DA, Nelson SJ, Vigneron DB, et al. A dual-tuned quadrature volume coil with mixed λ/2 and λ/4 microstrip resonators for multi-nuclear MRSI at 7 T. Magn Reson Imaging 2012;30:290–8.
[87] Svejda JT, Erni D, Rennings A. Near-field measurements and dual-tuned matching of two CDRA versions for combined 1H/23Na 7 T-MRI. Proc Intl German Microwave Conf 2016:104–7.
[88] Svejda JT, Rennings A, Erni D. A metamaterial based dual-resonant coil element for combined sodium/hydrogen MRI at 7 tesla. tm. Technisches Messen 2017;84:2–12.
[89] Svejda JT, Rennings A, Erni D. Compact metamaterial-based coil element for combined 1H/23Na MRI at 7T. Intl Conf Metamater Nanophoton 2019;4.
[90] Lee SW, Hilal SK, Cho ZH. A multinuclear magnetic resonance imaging technique – simultaneous proton and sodium imaging. Magn Reson Imaging 1986;4:343–50.
[91] Augath M, Heiler P, Kirsch S, Schad LR. In vivo 39K, 23Na and 1H MR imaging using a triple resonant RF coil setup. J Magn Reson 2009;200:134–6.
[92] Moon CH, Furlan A, Kim JH, Zhao T, Shapiro R, Bae KT. Quantitative sodium MR imaging of native versus transplanted kidneys using a dual-tuned proton/sodium (1H/23Na) coil: initial experience. Eur Radiol 2014;24:1320–6.
[93] Rutledge O, Kwak T, Cao P, Zhang X. Design and test of a double-nuclear RF coil for 1H MRI and 13C MRSI at 7T. J Magn Reson 2016;267:15–21.
[94] Hong S-M, Choi C-H, Magill AW, Shah NJ, Felder J. Design of a quadrature 1H/31P coil using bent dipole antenna and 4-channel loop at 3T MRI. IEEE Trans Med Imaging 2018;37:2613–8.
[95] Alfonsetti M, Sotgiu A, Alecci M. Design and testing of a 1.5 Tesla double-tuned (1H/31P) RF surface coil with intrinsic geometric isolation. Measurement 2010;43:1266–76.
[96] Yan X, Shi L, Wei L, Zhuo Y, Zhou XJ, Xue R, et al. A hybrid sodium/proton double-resonant transceiver array for 9.4T MRI. IEEE IMWS-BIO 2013:1–3. https://doi.org/10.1109/IMWS-BIO.2013.6756178.
[97] Ha Y, Choi C-H, Shah NJ. Development and implementation of a PIN-diode con-trolled, quadrature-enhanced, double-tuned RF coil for sodium MRI. IEEE Trans Med Imaging 2018;37:1626–31.
[98] Choi C-H, Ha Y, Magill AW, Shah NJ. Design of quadrature-compensated double-tuned RF surface coil using trap circuits. Proc Intl Soc Mag Reson Med 2016;24:2316.
[99] Klomp DW, Collins DJ, van den Boogert HJ, Schwarz A, Rijpkema M, Prock T, et al. Radio-frequency probe for 1H decoupled 31P MRS of the head and neck region. Magn Reson Imaging 2001;19:755–9.

[100] Du F, Liu S, Chen Q, Li N, Dou Y, Yang X, et al. Numerical simulation and evaluation of a four-channel-by-four-channel double-nuclear RF coil for 1 H MRI and31P MRSI at 7 T. IEEE Trans Magn 2018;54:1–5.

[101] Yan X, Xue R, Zhang X. A monopole/loop dual-tuned RF coil for ultrahigh field MRI. Quant Imaging Med Surg 2014;4:225.

[102] Han SD, Song J, Hernandez D, Kim K-N. Dual-tuned monopole/loop coil array for concurrent RF excitation and reception capability for MRI. J Kor Phys Soc 2019;75:610–6.

[103] Shajan G, Mirkes C, BVuckenmaier K, Hoffmann J, Pohmann R, Scheffler K. Three-layered radio frequency coil arrangement for sodium MRI of the human brain at 9.4T. Magn Reson Med 2016;75:906–16.

[104] Thapa B, Kaggie J, Sapkota N, Frank D, Jeong EK. Design and development of a general-purpose transmit/receive (T/R) switch for MRI, compatible for a linear, quadrature and double-tuned RF coil. Concepts Magn Reson B 2016;46:56–65.

[105] Adriany G, Gruetter R. A half-volume coil for efficient proton decoupling in hu-mans at 4 tesla. Magn Reson Med 1997;125:178–84.

[106] Li S, Zhang Y, Wang S, Yang J, Ferraris Araneta M, Farris A, et al. In vivo 13C Magnetic resonance spectroscopy of human brain on a clinical 3T scanner using [2-13C]Glucose infusion and low-power stochastic decoupling. Magn Reson Med 2009;62:565–73.

[107] Li S, An L, Yu S, et al. (13)C MRS of human brain at 7 Tesla using [2-(13)C]glucose infusion and low power broadband stochastic proton decoupling. Magn Reson Med 2016;75(3):954–61.

[108] Schaller B, Paritmongkol W, Rodgers CT. Quadrature 31P and single 1H dual-tune coil for cardiac 31P-MRS at 7T. Proc Intl Soc Mag Reson Med 2016;24:4006.

[109] Brunner DO, de Zanche N, Fröhlich J, Paska J, Puessmann KP. Traveling-wave nuclear magnetic resonance. Nature 2009;457:994–8.

[110] Mirkes C, Hoffmann J, Shajan G, Pohmann R, Scheffler K. High-resolution quantitative sodium imaging at 9.4 tesla. Magn Reson Med 2015;72:342–51.

[111] Schmidt R, Webb A. Characterization of an HEM-mode dielectric resonator for 7-T human phosphorous magnetic resonance imaging. IEEE Trans Biomed Eng 2016;63:2390–5.

[112] Choi C-H, Ha Y, Veeraiah P, Felder J, Moellonhoff K, Shah NJ. Development of a simple multinuclear MRI system for ultra-high field imaging of animals. J Magn Reson 2016;273:28–32.

[113] Gareis D, Neuberger T, Behr VC, Jakob PM, Faber C, Griswold MA. Transmit-receive coil-arrays at 17.6T, configurations for 1H, 23Na, and 31P MRI. Concepts Magn Reson B 2006;29:20–7.

[114] Fitzsimmons JR, Beck BL, Brooker HR. Double resonant quadrature birdcage. Magn Reson Med 1993;30:107–14.

[115] Fitzsimmons JR, Brooker HR, Beck BL. A transformer-coupled double-resonant probe for NMR imaging and spectroscopy. Magn Reson Med 1987;5:471–7.

[116] Asfour A. Design and development of a new dedicated RF sensor for the MRI of rat brain. J Biomed Sci Eng 2010;3:167–80.

[117] Hudson AMJ, Köckenberger W, Bowtell RW. Dual resonant birdcage coils for 1H detected13C microscopic imaging at 11.7 T. Magn Reson Mat Phys Biol Med 2000;10:61–8.

[118] Brand CJ, Webb AG, Beenakeer JWM. Design and performance of a transformer-coupled double resonant quadrature birdcage coil for localized proton and phos-phorus spectroscopy in the human calf muscle at 7T. Concepts Mag Reson B 2013;42:155–64.

[119] Brown R, Lakshmanan K, Madelin G, Parasoglou P. A nested phosphorus and proton coil array for brain magnetic resonance imaging and spectroscopy. Neuroimage 2016;124:602–11.

[120] Brown R, Khegai O, Parasoglou P. Magnetic resonance imaging of phosphocreatine and determination of BOLD kinetics in lower extremity muscles using a dual-fre-quency coil array. Sci Rep 2016;6:30568.

[121] Wiggins GC, Brown R, Fleysher L, Zhang B, Stoeckel B, Inglese M, et al. A nested dual frequency birdcage/stripline coil for sodium/proton brain imaging at 7T. Proc Intl Soc Mag Reson Med 2010;18:1500.

[122] Goluch G, Kuehne A, Meyerspeer M, et al. A form-fitted three channel 31P, two channel 1H transceiver coil array for calf muscle studies at 7 T. Magn Reson Med 2015;73:2376–89.

[123] Wang C, Li Y, Wu B, Xu D, Nelson SJ, Vigneron DB, et al. A practical multinuclear transceiver volume coil for in vivo MRI/MRS at 7 T. Magn Reson Imaging 2012;30:78–84.

[124] Kim JH, Moon CH, Park BW, Furlan A, Zhao T, Bae KT. Multichannel transceiver dual-tuned RF coil for proton/sodium MR imaging of knee cartilage at 3 T. Magn Reson Imaging 2012;30:562–71.

[125] Boehmert L, Kuehne A, Waiczies H, et al. Cardiorenal sodium MRI at 7.0 Tesla using a 4/4 channel (1) H/(23) Na radiofrequency antenna array. Magn Reson Med 2019;82:2343–56.

[126] Fantasia M, Galannte A, Maggiorelli F, Retico A, Fontana N, Monorchio A, et al. Numerical and workbench design of 2.35 T double-tuned (1H/23Na) nested RF birdcage coils suitable for animal size MRI. IEEE Trans Med Imaging 2020. https://doi.org/10.1109/TMI.2020.2988599.

[127] Lakshmanan K, Brown R, Madelin G, Qian Y, Boada F, Wiggins GC. An eight-channel sodium/proton coil for brain MRI at 3 T. NMR Biomed 2018;31:e3867.

[128] Avdievich NI, Peshkovsky AS, Hetherington HP. High-field double-tuned TEM/birdcage volume coil for human brain imaging. Proc Intl Soc Mag Reson Med 2007;15:239.

[129] S. Saha. Hybrid birdcage-TEM radio frequency (RF) coil for multinuclear MRI/MRS. US8035384B2. 2011.

[130] A.S. Peshkovsky. Dual-tuned TEM/birdcage hybrid volume coil for human brain and spectroscopy. US2008/0157770A1. 2008.

[131] Findeklee C, Leussler C, Morich M, Demeester G. Efficient design of a novel double tuned quadrature headcoil for simultaneous 1H and 31P MRI/MRS at 7T. Proc Intl Soc Mag Reson Med 2005;13:891.

[132] Dabirzadeh A, McDougall MP. Trap design for insertable second-nuclei radio-frequency coils for magnetic resonance imaging and spectroscopy. Concepts Magn Reson B 2009;35:121–32.

[133] Meyerspeer M, Roig ES, Gruetter R, Magill AW. An improved trap design for de-coupling multinuclear RF coils. Magn Reson Med 2014;72:584–90.

[134] Seres Roig E, Magill AW, Donati G, Meyerspeer M, Ipek O, Gruetter R. A double-quadrature radiofrequency coil design for proton-decoupled carbon-13 magnetic resonance spectroscopy in humans at 7T. Magn Reson Med 2015;73:894–900.

[135] Avdievich NI, Ruhm L, Dorst J, Scheffler K, Korzowski A, Henning A. Double-tunned 31P/1H human head array with high performance at both frequencies for spectroscopic imaging at 9.4T. Magn Reson Med 2020. https://doi.org/10.1002/mrm.28176.

[136] Alecci M, Romanzetti S, Kaffanke J, Celik A, Wegener HP, Shah NJ. Practical design of a 4 tesla double-tuned RF surface coil for interleaved 1H and 23Na MRI of rat brain. J Magn Reson 2006;181:203–11.

[137] Giovannetti G, Flori A, Marsigli F, et al. A radiofrequency system for in vivo hy-perpolarized 13C MRS experiments in mice with a 3T MRI clinical scanner. Scanning 2016;38:710–9.

[138] Brizi D, Fontana N, Costa F, Tiberi G, Galante A, Alecci M, et al. Design of dis-tributed spiral resonators for the decoupling of MRI double-tuned RF coils. IEEE Trans Biomed Eng 2020. https://doi.org/10.1109/TBME.2020.2971843.

[139] Malzacher M, Chacon-Caldera J, Paschke N, Schad LR. Feasibility study of a double resonant 8-channel 1H/8-channel 23Na receive-only head coil at 3 tesla. Magn Reson Imaging 2019;59:97–104.

[140] Lakshmanan K, Dehkharghani S, Madelin G, Brown R. A dual-tuned (17) O/(1) H head array for direct brain oximetry at 3 tesla. Magn Reson Med 2020. https://doi. org/10.1002/mrm.28005.

[141] Avdievich NI, Ruhm L, Dorst J, et al. Double-tuned 31P/1H human head array with high performance at both frequencies for spectroscopic imaging at 9.4T. Magn Reson Med 2020. https://doi.org/10.1002/mrm.28176.

[142] B.L. van de Bank, Orzada S, Smits F, Lagemaat MW, Rodgers CT, Bitz AK, et al. Optimized 31P MRS in the human brain at 7T with a dedicated RF coil setup. NMR Biomed 2015;28:1570–8.

[143] van Uden MJ, Peeters TH, Rijpma A, Rodgers CT, Heerschap A, Scheenen TWJ. An 8-channel receive array for improved (31) P MRSI of the whole brain at 3T. Magn Reson Med 2019;82:825–32.

[144] Rao M, Wild JM. RF instrumentation for same-breath triple nuclear lung MR imaging of 1H and hyperpolarized 3He and 129Xe at 1.5T. Magn Reson Med 2016;75:1841–8.

[145] Magill AW, Choi C-H, Ha Y, Shah NJ. Design and construction of a triple-tuned RF probe for 23Na/31P/1H using traps. Proc Intl Soc Magn Reson Med 2016;24:2135.

[146] Wiltshire MCK, Pendry B, Young IR, Larkman DJ, Gilderdale D, Hajnal JV. Microstructured magnetic materials for RF flux guides in magnetic resonance imaging. Science 2001;291:849–51.

[147] Zhao X, Duan G, Wu K, Anderson SW, Zhang X. Intelligent metamaterials based on nonlinearity for magnetic resonance imaging. Adv Mater 2019;31:1905461.

[148] Panda V, DelaBarre L, Adriany G, Vaughan JT, Gopinath A. Metamaterial zeroth-order resonator RF coil for human head: preliminary design for 10.5 T MRI. IEEE Journal of Electromagnetics, RF and Microwaves in Medicine and Biology. vol. 3. 2019. p. 33.

[149] Schmidt R, Slobozhanyuk A, Belov P, Webb A. Flexible and compact hybrid me-tasurfaces for enhanced ultra high field in vivo magnetic resonance imaging. Sci Rep 2017;7:1678.

[150] Dubois M, Vergara Gomez TS, Jouvaud C, et al. Enhancing surface coil sensitivity volume with hybridized electric dipoles at 17.2 T. J Magn Reson 2019;307:106567.

[151] Freire MJ, Jelinek L, Marques R, Lapine M. On the applications of $\mu_r = -1$ me-tamaterial lenses for magnetic resonance imaging. J Magn Reson 2010;203:81–90.

[152] Slobozhanyuk AP, Poddubny AN, Raaijmakers AJE, van den Berg CAT, Kozachenko AV, Dubrovina IA, et al. Enhancement of magnetic resonance imaging with metasurfaces. Adv Mater 2016;28:1832–8.

[153] Nikulin A, Ourir A, de Rosny J. Dual-tuned birdcage like coil based on meta-surfaces. Proc Intl Conf Days Diffract 2018:230–4.

[154] Hurshkainen A, Nikulin A, Georget E, et al. A novel metamaterial-inspired RF-coil for preclinical dual-nuclei MRI. Sci Rep 2018;8:9190.

[155] Vergara Gomez TS, Dubois M, Glybovski S, et al. Wireless coils based on resonnant and nonresonant coupled-wire structure for small animal multinuclear imaging. NMR Biomed 2019;32:e4079.

[156] Yang T, Ford KL, Rao M, Wild JM. A metasurface for multi-nuclear magnetic re-sonance imaging applications at 1.5 T. European Conference on Antenna and Propagation (EuCAP). 2019. p. 13.

[157] Ivanov VA, Hurshkainen A, Solomakha GA, Zubkov MA. RF-coil with variable resonant frequency for multiheteronuclear ultra-high field MRI. J Photon 2020;100747.

[158] Schmidt R, Webb A. Metamaterial combining electric- and magnetic-dipole-based configurations for unique dual-band signal enhancement in ultrahigh-field mag-netic resonance imaging. Appl Mater Interfaces 2017;9:34618–24.

[159] Roemer PR, Edelstein WA, Hayes CE, Souza SP, Mueller OM. The NMR phased array. Mag Reson Med 1990;16:192–225.

[160] von Morze C, Tropp J, Banerjee S, Xu D, Karpodinis K, Carvajal L, et al. An eight-channel, nonoverlapping phased array coil with capacitive decoupling for parallel MRI at 3 T. Concepts Mag Reson B 2007;31B(1):37–43.

[161] Avdievich NI, Pan JW, Hetherington HP. Resonant inductive decoupling (RID) for transceiver arrays to compensate for both reactive and resistive components of the mutual impedance. NMR Biomed 2013;26:1547–54.

[162] Zhang B, Sodickson DK, Cloos MA. A high-impedance detector-array glove for magnetic resonance imaging of the hand. Nat Biomed Eng 2018;2:570–7.
[163] Ruytenberg T, Webb A, Zivkovic I. Shielded-coaxial-cables as receive and trans-ceiver array elements for 7T human MRI. Mag Reson Med 2020;83:1135–46.
[164] Yan X, Gore JC, Grissom WA. Self-decoupled radiofrequency coils for magnetic resonance imaging. Nat Commun 2018;9:3481.
[165] Li Y, Xie Z, Pang Y, Vigneron D, Zhang X. ICE decoupling technique for RF coil array designs. Med Phys 2011;38:4086–93.
[166] Li N, Chen Q, Luo C, Lee J, Du F, Zhang ZX, et al. Investigation of a dual-tuned RF coil array decoupled using ICE technique for 1H/19F MR imaging at 3T. IEEE Trans Mag 2020;56:1–4.
[167] Yan X, Zhang X, Wei L, Xue R. Design and test of magnetic wall decoupling for dipole transmit/receive array for MR imaging at the ultrahigh field of 7T. Appl Magn Reson 2015;46:59–66.
[168] Mollaei MSM, Hurshkainen A, Kurdjumov S, Simovski C. Double-resonant de-coupling method in very dense dipole arrays. Photon Nanostruct Fundam Appl 2020;39:100767.
[169] Hurshkainen AA, Derzhavskaya TA, Glybovski SB, Voogt IJ, Melchakova IV, van den Berg CAT, et al. Element decoupling of 7T dipole body arrays by EBG meta-surface structures: experimental verification. J Magn Reson 2016;269:87–96.
[170] Gast LV, Henning A, Hensel B, Uder M, Nagel AM. Localized B0 shimming based on 23Na MRI at 7 T. Magn Reson Med 2020;83:1339–47.
[171] Nagel AM, Weber MA, Lehmann-Horn F, et al. Chlorine (35Cl) MRI in humans: cl-alterations do not correspond to disease-related Na+ changes. Proc Intl Soc Mag Reson Med 2013;21:116.
[172] Umathum R, Rösler MB, Nagel AM. In vivo 39K MR imaging of human muscle and brain. Radiology 2013;269:569–76.
[173] Anazodo UC, Farag A, Théberg J, et al. Assessment of PET performance of a 32-channel MR brain array head coil compatible with PET for integrated PET-MRI. Proc PSMR Conf 2016.
[174] Corea J, Ye P, Seo D, et al. Printed receive coils with high acoustic transparency for magnetic resonance guided focused ultrasound. Sci Rep 2018;8:3392.
[175] Rieke V, Ganguly A, Daniel BL, et al. X-ray compatible radiofrequency coil for magnetic resonance imaging. Magn Reson Med 2005;53:1409–14.
[176] Barta R, Ghila A, Rathee S, Fallone BG, De Zanche N. Low-attenuation RF surface coils for linac-MR hybrids compromise between radiation dose to the skin and SNR. Proc Intl Soc Mag Reson Med 2017;25:4435.
[177] Zijlema SE, Tijssen RHN, Malkov VN, et al. Design and feasibility of a flexible, on-body, high impedance coil receive array for a 1.5 T MR-linac. Phys Med Biol 2019;64:185004.
[178] Quick HH. Integrated PET/MR. J Magn Reson Imaging 2014;39:243–58.
[179] Oehmigen M, Lindemann ME, Gratz M, Neji R, Hammers A, Sauer M, et al. A dual-tuned (13) C/(1) H head coil for PET/MR hybrid neuroimaging: development, attenuation correction, and first evaluation. Med Phys 2018;45:4877–87.
[180] Choi C-H, Tellmann L, Felder J, Lerche C, Shah NJ. An evaluation of RF coil materials for 1H/31P for use in a hybrid MR-PET scanner at 3T. Proc Intl Soc Mag Reson Med 2017;25:4432.
[181] Sander CY, Keil B, Chonde DB, Rosen BR, Catana C, Wald LL. A 31-channel MR brain array coil compatible with positron emission tomography. Magn Reson Med 2014;73:2363–75.
[182] Farag A, Thompson RT, Thiessen JD, et al. Assessment of a novel 32-channel phased array for cardiovascular hybrid PET/MRI imaging: MRI performance. Eur J Hybrid Imaging 2019;3:13.
[183] Choi C-H, Felder T, Felder J, Tellmann L, Hong S-M, Wegener H-P, et al. Design, evaluation and comparison of endorectal coils for hybrid MR-PET imaging of the prostate. Phys Med Biol 2020;65:115005.